

Introduction to IBIS-ArcSAR: a circular scanning GB-SAR system for deformation monitoring

Alberto Michellini¹, Federico Viviani¹, Lorenzo Mayer¹

¹IDS GeoRadar, Via Augusto Righi 1-2, 56121, Pisa, Italy (alberto.michellini@idsgeoradar.com)

Key words: GB-SAR; Interferometry; Radar Imaging; Geohazard monitoring; Open pit mine monitoring

ABSTRACT

In the last decade, Ground-Based Synthetic Aperture Radar (GB-SAR) Interferometry has become a well-established technique for deformation monitoring of several scenarios, including landslides, glaciers, dams and open pit mines. This goal has been achieved thanks to the GB-SAR specific advantages, such as remote sensing, high sensitivity to small deformations, long range of measurements, imaging capability and fast scan time.

The GB-SAR systems synthesize an aperture along azimuth direction by moving the radar head on a linear rail while transmitting a Frequency Modulated Continuous Wave (FMCW) signal. A 2D range-azimuth image can be produced through proper signal processing, and repeated acquisitions in time of the same scenario can be processed through differential interferometry techniques, obtaining 2D range-azimuth displacements maps.

However, especially in open pit mine geometries, the 80° azimuth field of view of a typical GB-SAR system can be a limiting factor in comparison to other monitoring technologies (e.g. Real Aperture Radar). Recently, to overcome this limit, IDS GeoRadar developed IBIS-ArcSAR: an innovative circular scanning GB-SAR system with 360° horizontal coverage capability, with constant angular resolution.

In this paper the differences between the standard linear scan and the new circular scan applied to GB-SAR systems are reviewed; in particular differences in focusing techniques, antenna pattern role and the focused 2D image properties, are analyzed. Then the IBIS-ArcSAR system is presented, describing the hardware setup and the technological solutions implemented to improve GB-SAR systems' performances. Finally, various real dataset results, acquired during the last year, are reported and analyzed.

I. INTRODUCTION

Interferometric Ground-Based Synthetic Aperture Radar (GB-SAR) is a class of remote sensing systems able to provide 2D images and to estimate small displacements, exploiting differential interferometry techniques (Monserrat *et al.* 2014), (Caduff *et al.* 2015). These systems have been widely used in many deformation monitoring environments, such as landslides (Herrera *et al.* 2009), (Mazzanti *et al.* 2015), glaciers (Noferini *et al.* 2009), (Dematteis *et al.* 2017), urban sites (Pipia *et al.* 2007), (Crosetto *et al.* 2014), open pit mines (Atzeni *et al.* 2015), (Ramsden *et al.* 2015), bridges (Gentile *et al.* 2008), (Kuras *et al.* 2012) and dams (Alba *et al.* 2008), (Di Pasquale *et al.* 2018).

Common GB-SAR systems realize a synthetic aperture by moving a radar sensor on a rail while transmitting a Frequency Modulated Continuous Wave (FMCW) signal. Starting from the raw data acquired, a 2D range-azimuth complex-valued image is obtained through a proper focusing; repeating the SAR acquisition at various times and applying differential interferometry techniques, a 2D Line of Sight (LoS) displacement map can be computed (Rödelsperger 2011). Then, knowing the radar position, it is possible to back-project the 2D radar images onto a Digital Terrain Model (DTM) obtaining a valuable 3D representation of the deformation scenario (Figure 1).

One of the main limitations of common GB-SAR with respect to other technologies, as for example Real Aperture Radar (RAR) (Pieraccini 2013), is the limited horizontal Field of View (FoV), which is bounded by the antennas horizontal beamwidth to about 80°. Such horizontal FoV is usually not a problem for remote monitoring of landslides and glaciers, but it may become a relevant limitation in open cast mining environment, where a reduced horizontal coverage turns out in a smaller covered area, because of the pit circular geometry.

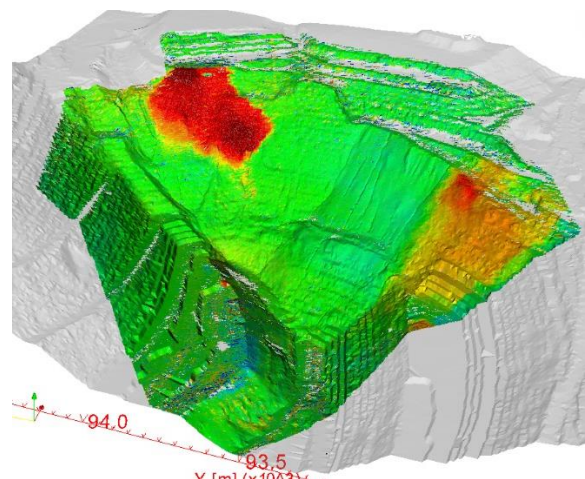


Figure 1. Typical GB-SAR Geocoded displacement map

To increase the GB-SAR FoV, in the past various circular scanning prototypes have been proposed and tested (Lee *et al.* 2014), (Luo *et al.* 2014), (Pieraccini *et al.* 2017) and (de Macedo *et al.* 2017) but none of them has been subsequently developed to become a fully engineered system. Recently IDS GeoRadar has developed IBIS-ArcSAR: an innovative circular scanning GB-SAR system with the capability to synthesize images at 360° with constant angular resolution and with an improved level of engineering compared to the other GB-SAR systems on the market (Viviani *et al.* 2017).

In this paper the differences between the standard linear scan and the new circular scan applied to GB-SAR systems are presented. In particular in section II some SAR imaging concept are reviewed and applied, first to the linear case (II.A), then to the circular case (II.B). In section III the IBIS-ArcSAR system is presented, first describing the hardware setup and some of the technological solutions implemented (III.A), then in section III.B two real dataset results, acquired during the last year, are reported and discussed, with particular focus on the new wide coverage introduced by the circular scanning.

II. SAR IMAGING

Unlike the optical or the RAR imagery, SAR data have to be pre-processed in order to obtain an exploitable image; this procedure is commonly called image focusing. SAR focusing is usually a 2D problem, in which the effects of frequency modulation and those of system motion are processed simultaneously. Since this paper analyzes the differences between linear and circular scanning, only the system motion effects will be considered in the following, in this way the focusing will be reduced to a 1D problem.

Generally speaking, a SAR acquisition can be labelled by a set of parameters \mathbf{p} as for examples the acquisition time, the position along a rail or the position on a curvilinear orbit. The generation of any SAR image starts with a raw data d , that is essentially what the sensor acquires during the acquisition, and that can be represented by a complex valued function $d(\mathbf{p})$ of the SAR acquisition parameters (Figure 2).

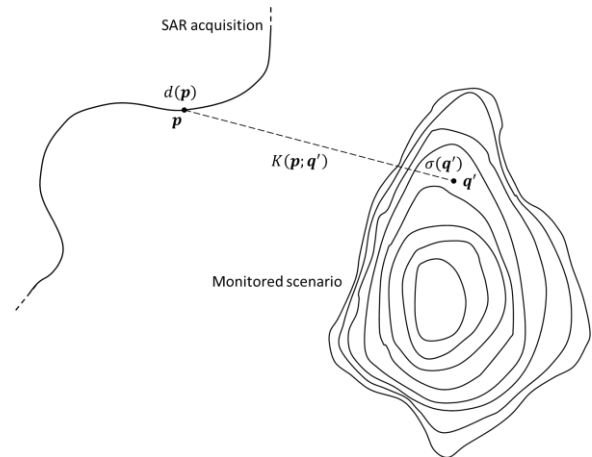


Figure 2. SAR acquisition model

The scenario measured by a SAR system is usually described by a microwave backscattering coefficient that can be represented by a complex function $\sigma(\mathbf{q})$ defined on an ambient space Q as for example the common three-dimensional Euclidean space. Given a target located in the position $\mathbf{q}' \in Q$, SAR raw data are connected to the target reflectivity through a kernel $K(\mathbf{p}; \mathbf{q}')$ that keeps in account of the various Radar propagation factors (Bamler *et al.* 1998), (Dickey *et al.* 2001):

$$d(\mathbf{p}) = \int K(\mathbf{p}; \mathbf{q}') \sigma(\mathbf{q}') d\mathbf{q}' \quad (1)$$

Therefore, in the SAR raw data, the signal energy from a point target is distributed across all the SAR acquisition, and the purpose of image focusing is to collect this scattered energy into a single pixel in the output image.

Starting from (1) it is possible to compute a SAR focused image $s(\mathbf{q})$ evaluated in the position $\mathbf{q} \in Q$, multiplying the SAR raw data by a complex steering vector $H(\mathbf{q}; \mathbf{p})$ and then integrating along SAR acquisition parameters (2).

$$s(\mathbf{q}) = \int H(\mathbf{q}; \mathbf{p}) d(\mathbf{p}) d\mathbf{p} \quad (2)$$

Thanks to linearity of (1) and (2), the resulting focused image can be expressed as a convolution between the target reflectivity and the system Point Spread Function (PSF) $\chi(\mathbf{q}; \mathbf{q}')$ (3) that describes, as a function of \mathbf{q} , the SAR imaging system response to a point source located in \mathbf{q}' .

$$s(\mathbf{q}) = \int \chi(\mathbf{q}; \mathbf{q}') \sigma(\mathbf{q}') d\mathbf{q}' \quad (3)$$

The analysis of the PSF of an imaging system allows the determination of various parameters, in particular in Radar imaging are considered, among others, the Peak Side Lobe Ratio (PSLR) and the spatial resolution

The PSLR is defined by the ratio between the strongest level of PSF sidelobes to the PSF main lobe peak level. It represents the ability of the imaging system to identify a weak target from a nearby strong

one. In fact, sidelobes from large targets can obscure signals coming from nearby smaller targets.

The spatial resolution instead represents the ability of the imaging system to distinguish two close similar targets; in Radar imaging, it is usually measured by the distance between the points with intensities 3 dB below the PSF main lobe peak level.

In the SAR focused image, combining (1) and (2) it is possible to express the PSF as a convolution between the system kernel K and the focusing steering vector H :

$$\chi(\mathbf{q}; \mathbf{q}') = \int H(\mathbf{q}; \mathbf{p})K(\mathbf{p}; \mathbf{q}')d\mathbf{p} \quad (4)$$

It is well known (Chan *et al.* 2008) that matched steering vector $H(\mathbf{q}; \mathbf{p}) = K^*(\mathbf{p}; \mathbf{q})$ maximize the target Signal to Noise Ratio (SNR) or equivalently it maximizes the PSF main lobe peak respect to the noise level; in physical systems, however, the aperture finiteness inevitably causes undesirable sidelobes in the PSF. SAR sidelobes, may be reduced by exploiting window taper functions $W(\mathbf{p})$ across the finite aperture, albeit at the expense of other parameters degradations such as the spatial resolution (Doerry 2017).

In the next two sections, these general concepts will be applied to the specific cases of linear and circular GB-SAR

A. Linear GB-SAR

Currently, the most common GB-SAR configuration exploited for deformation monitoring is the linear one. A generic linear GB-SAR system is composed by a Radar sensor that moves along a linear rail of length L (Monserat *et al.* 2014), (Farina *et al.* 2011). Consider a Cartesian coordinate system (x, y, z) with the origin placed at the center of the rail and oriented in order to have the SAR scan directed along the positive x axis and the vertical direction along the positive z axis. With this convention the linear GB-SAR acquisition can be labelled by the parameter $p = x/L$ that goes from $-1/2$ to $1/2$.

Thanks to the system axial symmetry around the scan direction, it is natural to define a spherical coordinate system (r, θ_l, ϕ_l) as in Figure 3, where r is the distance from the coordinate system origin, θ_l is the elevation angle or look-angle and ϕ_l is the azimuth angle. The subscript l helps to distinguish these angles from those that will be defined for the circular case, to which they tend in the small angles limit.

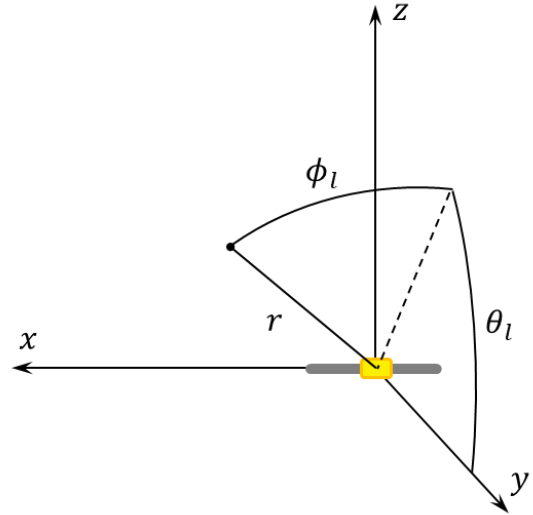


Figure 3. Linear GB-SAR geometry

With this convention, given a SAR position labelled by p it is possible to express the distance $r(p)$ between the SAR position and a point with spherical coordinates (r, θ_l, ϕ_l) as:

$$r(p) = \sqrt{(L \cdot p - r \sin \phi_l)^2 + r^2 \cos^2 \phi_l} \quad (5)$$

Consider now a linear GB-SAR system with a central wavelength λ and an antenna pattern $G(\theta_l, \phi_l)$, that aims an acquisition scenario described by a backscattering coefficient $\sigma(\theta_l, \phi_l)$. After range focusing, the raw data d received at the SAR position p can be expressed as

$$d(p) = \iint e^{-i\frac{4\pi}{\lambda}r(p)} G^2(\theta'_l, \phi'_l) \sigma(\theta'_l, \phi'_l) d\theta'_l d\phi'_l = \iint K_l(p; \theta'_l, \phi'_l) \sigma(\theta'_l, \phi'_l) d\theta'_l d\phi'_l \quad (6)$$

Where it has been introduced the linear GB-SAR kernel $K_l(p; \theta_l, \phi_l)$ which, in the far field region ($r > L^2/\lambda$), can approximate as

$$K_l(p; \theta_l, \phi_l) \simeq e^{-i\frac{4\pi}{\lambda}r} e^{i\frac{4\pi L}{\lambda}p \sin \phi_l} G^2(\theta_l, \phi_l) \quad (7)$$

Directly from this expression, some properties of the corresponding SAR imaging, can be deduced: first, the radiation pattern contribution is separated from the SAR position dependence, therefore the antennas will have no effect on the focusing procedure; secondly the azimuth angle is connected to the SAR position parameter through the sine function, indicating that the angular resolution is not azimuth independent but will vary as $\cos^{-1} \phi_l$; finally the kernel phase, does not depend on the elevation angle, therefore the knowledge of the scenario topography is not necessary to carry out the focusing.

As discussed before, focused data relative to the direction ϕ_l is obtained multiplying the raw data $d(p)$ by a steering vector $H_l(p; \phi_l)$ and integrating along SAR positions. In this case the generic steering vector is

given by the matched one multiplied by a window taper function:

$$H_l(\phi_l; p) = W(p)e^{-i\frac{4\pi L}{\lambda}p \sin \phi_l} \quad (8)$$

Considering for example a window taper function that guarantees a 26 dB PSLR, it is possible to show from simple simulation (Figure 4) that the corresponding azimuth resolution $\delta\phi_l$ is the usual

$$\delta\phi_l = \frac{\lambda}{2L \cos \phi_l} \quad (9)$$

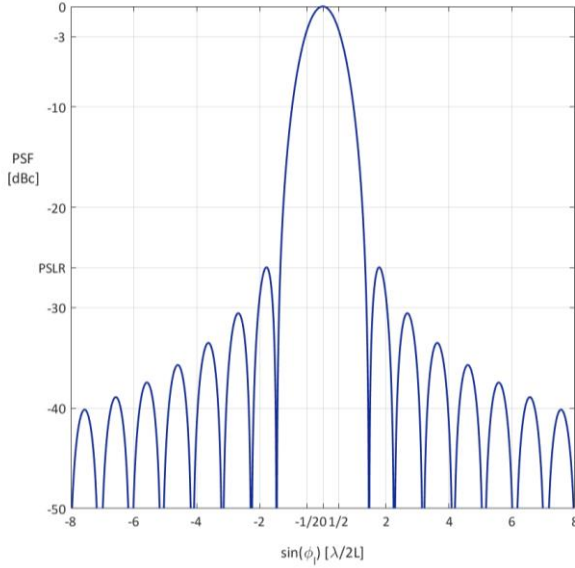


Figure 4. PSF of a linear GB-SAR with a 26 dB PSLR

B. Circular GB-SAR

After reviewing the basic concepts of the linear GB-SAR imaging, it is possible to extend them to the circular scan case. Generic circular GB-SAR system is composed by a radar sensor that moves on the xy plane along a circle of radius R , thus consider a Cartesian coordinate system (x, y, z) with the origin placed at the centre of the SAR rotation and oriented in order to have the axis of rotation directed along the positive z (Figure 5)

Thanks to the system axial symmetry around the rotation axis, it is also possible to define a spherical coordinate system (r, θ_c, ϕ_c) as in Figure 5 and the SAR scan positions can be labelled by the parameter $p = \phi_c/2\pi$ that goes from $-1/2$ to $1/2$. Given a point inside the monitored scenario it is possible to express the distance $r(p)$ between the target and a SAR position labelled by p as

$$r(p) = \sqrt{r^2 - 2rR \cos \theta_c \cos(2\pi p - \phi_c) + R^2} \quad (10)$$

Analogously to the linear case, consider now a circular GB-SAR system with a central wavelength λ and an antenna pattern $G(\theta_c, \phi_c)$, that aims an acquisition scenario described by a backscattering coefficient $\sigma(\theta_c, \phi_c)$. After range focusing, the raw data d received at the SAR position p can be expressed as

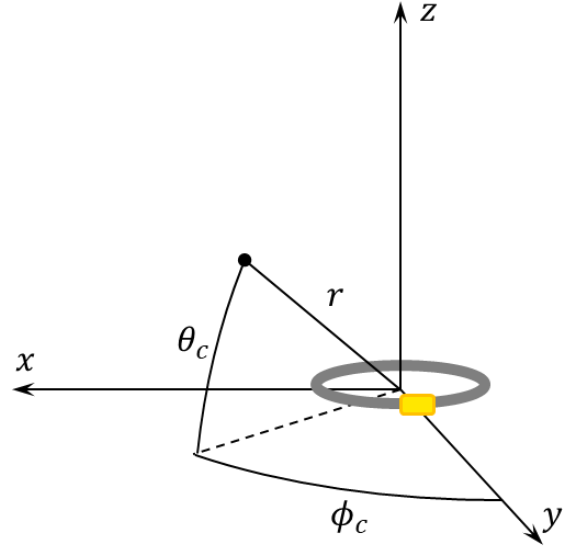


Figure 5. Circular GB-SAR geometry

$$d(p) = \iint e^{-i\frac{4\pi}{\lambda}r(p)} G^2(\theta'_c, \phi'_c - 2\pi p) \sigma(\theta'_c, \phi'_c) d\theta'_c d\phi'_c = \iint K_c(p; \theta'_c, \phi'_c) \sigma(\theta'_c, \phi'_c) d\theta'_c d\phi'_c \quad (11)$$

Where it has been introduced the circular GB-SAR kernel $K_c(p; \theta'_c, \phi'_c)$ which in the far field region ($r > R^2/\lambda$) can approximate as

$$K_c(p; \theta_c, \phi_c) = e^{i\frac{4\pi}{\lambda}R \cos \theta_c \cos(\phi_c - 2\pi p)} G^2(\phi_c - 2\pi p, \theta_c) \quad (12)$$

Also in this case, it is possible to deduce some SAR imaging properties directly from the kernel expression: first, because of the antenna rotation, the radiation pattern contribution is not anymore a multiplying factor but is convoluted with the SAR position parameter, acting as an analogical window taper function, and focusing procedure will depend on the antennas characteristics. Secondly the azimuth angle is connected linearly to the SAR position parameter, indicating that the angular resolution is constant, as expected from a circular scan. Finally the kernel phase depends also on the elevation angle θ_c , therefore it is necessary to have a certain knowledge of the scenario topography to carry out properly the focusing.

As before, data focusing along the direction ϕ_c is obtained by multiplying the received signal by a steering vector $H_c(\phi_c, \theta_c; p)$ and integrating along SAR positions. In this case, because of the antenna contribution, the matched steering vector contains already a window taper function $W = G^2$ given by the antenna radiation pattern. In this case, it is possible to focus the SAR image directly with the matched steering vector

$$H_c(\phi_c, \theta_c; p) = G^2(\phi_c - 2\pi p, \theta_c) e^{-i\frac{4\pi}{\lambda}R \cos \theta_c \cos(\phi_c - 2\pi p)} \quad (13)$$

To compare the circular PSF to the linear one, it is possible to select an appropriate antenna pattern and the correspondent steering vector, to obtain a 26 dB PSLR; the simulation shows that also in the circular case the corresponding azimuth resolution is the usual one for the circular SAR (Pieraccini *et al.* 2017):

$$\delta\phi_c = \frac{\lambda}{4R \sin \frac{\phi_{BW}}{2}} \quad (14)$$

Where ϕ_{BW} is the antenna azimuth beamwidth.

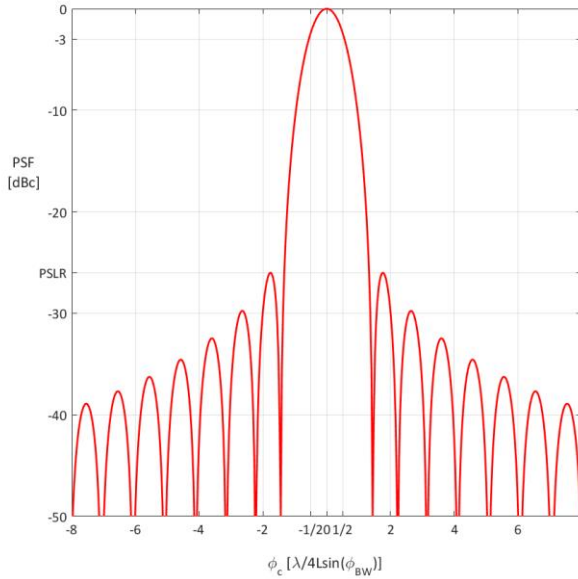


Figure 5. PSF of a circular GB-SAR with a 26 dB PSLR

III. IBIS-ARCSAR SYSTEM

IBIS-ArcSAR is a recently developed circular GB-SAR system by IDS GeoRadar; this innovative system has been conceived to bring in the mining industry 360° pit coverage capabilities from one single equipment. The Hardware and Software architecture have been designed for fast deployment and robustness, to ensure the highest operating standards even in a complex environment such as the mining one. The system technical specifications are resumed in Table 1.

In this section IBIS ArcSAR system is described and some real datasets are presented and discussed.

Table 1. IBIS-ArcSAR specification

Column 1	
Wavelength	17.43 mm
Power transmitted	≤ 20 dBm
Range resolution	37.5 cm
Azimuth resolution	4.3 mrad
Operative range	5 km
Azimuth FoV	360°
Elevation FoV	60°
Scan time	360° in 40s

A. System hardware description

IBIS-ArcSAR hardware basically consists of an interferometric radar sensor moved by a rotating mechanical arm, all positioned on a mobile trailer equipped with a built-in power supply system that, combined with a total power consumption of less than 100 W, guarantees the autonomy of the whole system (Figure 7)



Figure 7. IBIS ArcSAR system hardware overview

Compared to current GB-SAR systems, the major innovations introduced by IBIS-ArcSAR, reside in the arm-sensor module, that, in addition to the new scanning mode, integrates two GNSS antennas, a High-Definition (HD) camera, and two additional Radar channels, connected to two horn antennas. (Figure 8)

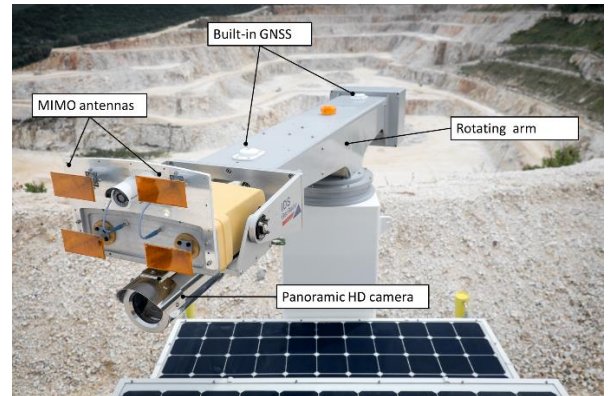


Figure 8. IBIS ArcSAR HW description

The two GNSS antennas are separated by a 1.3 m baseline and connected to a dual-frequency, dual-antenna GNSS receiver that allows the automatic measurement of system position and orientation with better accuracy than the system spatial resolution (Table 1). This integration considerably simplifies the geocoding procedure of the radar data, which is currently carried out manually by the GB-SAR users. The HD camera is a 16 Megapixel (MP) camera with 34°x49° field of view, that moves jointly with the sensor, taking several pictures during the circular scan. Once all the photos have been acquired, it is possible to process them with photo-stitching techniques to obtain a single

360°x49° field of view panoramic image, large up to 180 MP.

The two additional radar channels (one transmitter and one receiver) allow to acquire, in Multiple Input Multiple Output (MIMO) mode, four data streams at different baselines with a total 150 mm height. In this way, with only one SAR acquisition it is possible to estimate the scenario topography with no atmospheric contribution to the interferometric phase (Noferini *et al.* 2007), and use this information to perform both the focusing stage and the DTM reconstruction of the acquired scenario at low computational cost (Viviani *et al.* 2018).

B. Data Analysis

In this section two real IBIS-ArcSAR datasets are presented and discussed, with particular attention to the system's ability to acquire large FoV images.

The first scenario considered is an open pit gold mine with a diameter of about 2 km. IBIS-ArcSAR was deployed around halfway down the pit slope allowing to acquire relevant signals over all 360° of the circular scan, and to identify about 520'000 Permanent Scatterers (PS) (Ferretti *et al.* 2001) in the SAR image (Figure 9).

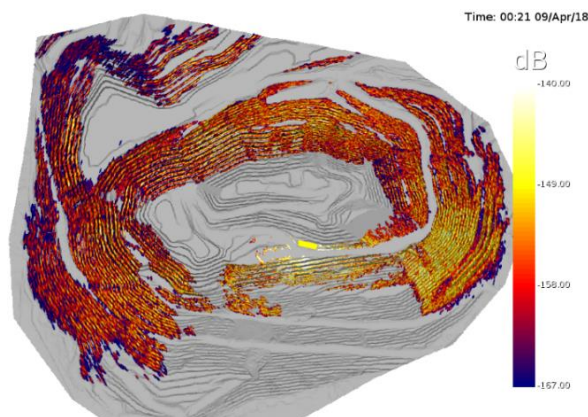


Figure 9. First scenario - Geocoded Power map

To better quantify the quality of interferometric data, temporal coherence was computed over a subset of 61 consecutive images, corresponding to 2h of continuous monitoring (Figure 10). The result indicates that more than 90% of the selected PS have a temporal coherence greater than 0.9, while about 40% of the PS have a temporal coherence even greater than 0.995, equivalent to a deformation measurement precision better than 0.1 mm (Just *et al.* 1994).

Starting from this data quality it is possible to obtain excellent results of the interferometric processing, which can be used by mine geotechnics in the form of displacement or velocity maps. As an example, in Figure 11 is shown the geocoded velocity map computed over a 24 h interval. The area subject to deformation, is clearly visible and identifiable within the pit. Moreover, the velocity of every PS is precisely

reported, allowing the application of geohazard alarms based on deformation rates.

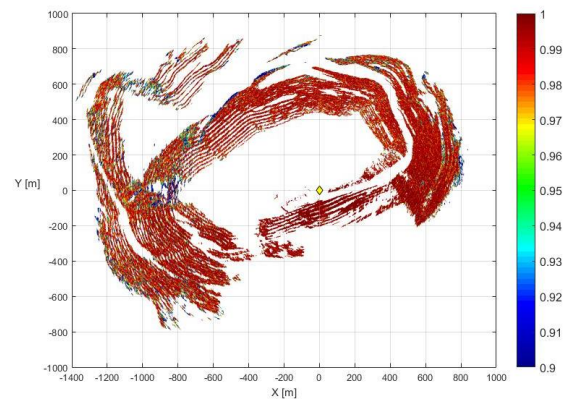


Figure 10. First scenario - Temporal coherence map computed over 61 consecutive acquisitions.

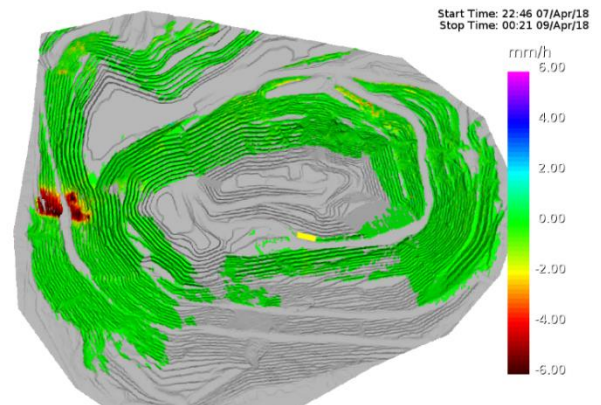


Figure 11. First scenario - Geocoded Velocity map

The second scenario considered is an open pit gold mine with a diameter of about 1.5 km; in this case IBIS-ArcSAR was deployed on one side of the pit, in order to cover the whole opposite slope inside a 150° FoV. The peculiarity of this dataset is that it contains a large moving area, occupying an angular sector greater than 40°. In these particular conditions, the IBIS-ArcSAR broad coverage allows to measure, together with the moving PS, a considerable number of stable PS which in turn allows a more effective atmospheric compensation. To better illustrate this concept, it is useful to consider Figure 12, where a raw interferogram is reported. Analyzing the interferometric phase only in the azimuth central sector, it would be difficult to distinguish the atmospheric contribution from that due to the real deformation. On the other hand, considering the phase globally, it is not complicated to distinguish the linear varying atmospheric contribution from the strongly non-linear deformation, and thus compensate the Atmospheric Phase Screen over the whole interferogram (Figure 13)

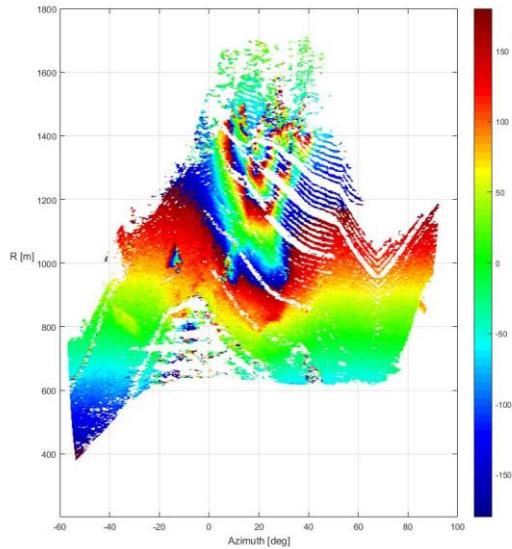


Figure 12. Second scenario - Raw interferogram in Polar coordinates

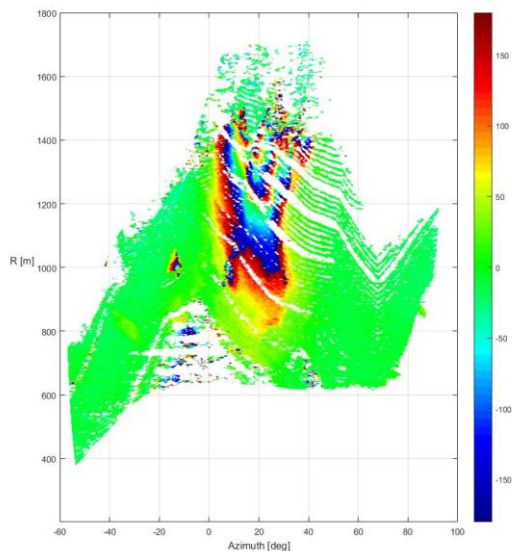


Figure 13. Second scenario - Compensated interferogram in Polar coordinates

IV. CONCLUSIONS

In this paper we have presented IBIS-ArcSAR, a new circular scanning GB-SAR system, developed to extend the FoV of the usual linear GB-SAR. This innovation has been proved to be extremely profitable, especially in open cast mining environment, where it allows an adequate coverage of the entire pit and it can help to improve the atmospheric compensation processing.

References

- Alba, M., G. Bernardini, A. Giussani, P. P. Ricci, F. Roncoroni, M. Scaioni, P. Valgoi, and Zhang, K. (2008) Measurement of dam deformations by terrestrial interferometric techniques. *Int. Arch. Photogramm. Remote Sens. Spat. Inf. Sci*, 37, 133-139.
- Atzeni, C., M. Barla, M. Pieraccini, and F. Antolini, (2015) Early warning monitoring of natural and engineered slopes with ground-based synthetic-aperture radar. *Rock Mechanics and Rock Engineering*, 48(1), 235-246.
- Bamler, R., and P. Hartl, (1998) Synthetic aperture radar interferometry. *Inverse problems*, 14(4), R1.
- Caduff, R., F. Schlunegger, A. Kos, and A. Wiesmann, (2015) A review of terrestrial radar interferometry for measuring surface change in the geosciences *Earth Surf. Process. Landforms*, 40, 208-228.
- Chan, Y. K., and V. C. Koo, (2008). An introduction to synthetic aperture radar (SAR). *Progress In Electromagnetics Research*, 2, 27-60.
- Crosetto, M., O. Monserrat, G. Luzi, M. Cuevas-González, and N. Devanthery, (2014) Discontinuous GBSAR deformation monitoring. *ISPRS Journal of Photogrammetry and Remote Sensing*, 93, 136-141.
- Doerry, A. W. (2017). Catalog of window taper functions for sidelobe control. *Sandia National Laboratories*, Albuquerque, New Mexico, USA.
- Dematteis, N., G. Luzi, D. Giordan, F. Zucca, and P. Allasia, (2017) Monitoring Alpine glacier surface deformations with GB-SAR. *Remote Sensing Letters*, 8(10), 947-956.
- Di Pasquale, A., G. Nico, A. Pitullo, and G. Prezioso, (2018) Monitoring strategies of earth dams by ground-based radar interferometry: How to extract useful information for seismic risk assessment. *Sensors*, 18(1), 244.
- Dickey, F. M., L. A. Romero, A. W. Doerry, (2001) Superresolution and synthetic aperture radar. Sandia Report, SAND2001-1532, *Sandia National Laboratories*, Albuquerque, NM, 87185.
- Farina, P., Leoni, L., Babboni, F., Coppi, F., Mayer, L. and Ricci, P. (2011) IBIS-M, an innovative radar for monitoring slopes in open-pit mines *Proc. Int. Symp. Rock Slope Stabil. Open Pit Mining Civil Eng.*
- Ferretti, A., Prati, C., and Rocca, F. (2001). Permanent scatterers in SAR interferometry. *IEEE Transactions on geoscience and remote sensing*, 39(1), 8-20.
- Gentile, C., and G. Bernardini, (2008) Output-only modal identification of a reinforced concrete bridge from radar-based measurements. *Ndt & E International*, 41(7), 544-553.
- Herrera, G., J. A. Fernández-Merodo, J. Mulas, M. Pastor, G. Luzi, and O. Monserrat, (2009) A landslide forecasting model using ground based SAR data: The Portalet case study. *Engineering Geology*, 105(3-4), 220-230.
- Just, D. and Bamler, R. (1994). Phase statistics of interferograms with applications to synthetic aperture radar. *Applied optics*, 33(20), 4361-4368.
- Kuras, P., T. Owerko, Ł. Ortyl, R. Kocierz, O. Sukta, and S. Pradelok, (2012). Advantages of radar interferometry for assessment of dynamic deformation of bridge. In *6th International Conference on Bridge Maintenance, Safety and Management (IABMAS 2012)*, Stresa, Lake Maggiore (pp. 885-891).

- Lee, H., Lee, J. H., Kim, K. E., Sung, N. H., and Cho, S. J. (2014). Development of a truck-mounted arc-scanning synthetic aperture radar. *IEEE Transactions on Geoscience and Remote Sensing*, 52(5), 2773-2779.
- Luo, Y., Song, H., Wang, R., Deng, Y., Zhao, F., and Xu, Z. (2014). Arc FMCW SAR and applications in ground monitoring. *IEEE Transactions on Geoscience and Remote Sensing*, 52(9), 5989-5998.
- de Macedo, K. A. C., Ramos, F. L. G., Gaboardi, C., Moreira, J. R., Vissirini, F., and da Costa, M. S. (2017). A compact ground-based interferometric radar for landslide monitoring: The xerém experiment. *IEEE Journal of Selected Topics in Applied Earth Observations and Remote Sensing*, 10(3), 975-986.
- Mazzanti, P., F. Bozzano, I. Cipriani, and A. Prestininzi, (2015) New insights into the temporal prediction of landslides by a terrestrial SAR interferometry monitoring case study. *Landslides*, 12(1), 55-68.
- Monserat, O., M. Crosetto, and G. Luzi. (2014) A review of ground-based SAR interferometry for deformation measurement. *ISPRS Journal of Photogrammetry and Remote Sensing*, vol. 93, pp. 40-48, Jul. 2014.
- Noferini, L., M. Pieraccini, D. Mecatti, G. Macaluso, G. Luzi, and C. Atzeni, (2007) DEM by ground-based SAR interferometry. *IEEE Geoscience and Remote Sensing Letters*, 4(4), 659-663.
- Noferini, L., D. Mecatti, G. Macaluso, M. Pieraccini, and C. Atzeni, (2009) Monitoring of Belvedere Glacier using a wide angle GB-SAR interferometer. *Journal of Applied Geophysics*, 68(2), 289-293.
- Pieraccini, M. (2013) Real beam vs. synthetic aperture radar for slope monitoring *Proc. Prog. Electromagn. Res. Symp.(PIERS)*, 1627-1630.
- Pieraccini, M., and Miccinesi, L. (2017) ArcSAR: Theory, simulations, and experimental verification. *IEEE Transactions on Microwave Theory and Techniques*, 65(1), 293-301.
- Pipia, L., X. Fabregas, A. Aguasca, C. Lopez-Martinez, J. J. Mallorqui, and O. Mora, (2007) A subsidence monitoring project using a polarimetric GB-SAR sensor. In *Workshop POLinSAR* (Vol. 1, pp. 22-26).
- Ramsden F., N. Coli, A. I. Benedetti, A. Falomi, L. Leoni and A. Michelini (2015) Effective use of slope monitoring radar to predict a slope failure at Jwaneng Mine, Botswana. In *Slope Stability 2015*, The Southern African Institute of Mining and Metallurgy. Cape Town, South Africa, 12-14 October 2015.
- Rödelsperger, S. (2011) Real-time processing of ground based synthetic aperture radar (GB-SAR) measurements (No. 33). *Technische Universität Darmstadt, Fachbereich Bauingenieurwesen und Geodäsie*.
- Viviani, F., Michelini, A., Mayer, L., and Coppi, F. (2018) IBIS-ArcSAR: an Innovative Ground-Based SAR System for Slope Monitoring. In *IGARSS 2018-2018 IEEE International Geoscience and Remote Sensing Symposium* (pp. 1348-1351). IEEE.